Check for updates

Elasticity promotes directional transport of *Pseudomonas aeruginosa* in native human airway mucus and complex fluids†

Riley Dickson,[b] Zhi-Jian He[c] and Li-Heng Cai ★[abcd]

Pseudomonas aeruginosa is an opportunistic bacterium that is readily cleared by mucus clearance in healthy individuals but becomes infectious in patients with mucus obstructive lung diseases, which are characterized by the formation of bacterial colonies or biofilms. The motility of *P. aeruginosa* is critical for biofilm formation, but it remains poorly understood how the bacterium transports within native mucus. Existing studies on mucus-bacteria interactions and *P. aeruginosa* transport within mucus largely rely on reconstituted mucus or purified mucins, which have properties dramatically different from native mucus. Here, we report the transport of *P. aeruginosa* strain PA14, a human clinical isolate responsible for chronic lung infections, in normal and diseased native human airway mucus. We use well-differentiated human bronchial epithelial cells cultured at the air–liquid-interface to secrete and harvest native human airway mucus with concentrations matching health and disease states. Furthermore, we develop a droplet-in-oil system for quantifying the transport of individual bacterium within bulk mucus. Remarkably, highly viscoelastic normal mucus promotes directional bacterial motility at a speed comparable to that in a low-viscosity physiological buffer. By contrast, concentrated, pathological mucus with elasticity dominating viscosity traps bacteria, reducing their motility more than 10-fold. Engineering mucus simulants with decoupled viscosity and elasticity reveals that the elasticity of complex fluids induces a qualitative change of bacterial motility from circular to directional motion. Our discovery not only provides insights into the biophysical mechanisms of bacterial infection in the lung but also reveals the previously unrecognized importance of elasticity in directional bacterial transport within complex fluids.

a Soft Biomatter Laboratory, Department of Materials Science and Engineering, University of Virginia, 228 Wilsdorf Hall, 395 McCormick Road, Charlottesville, VA 22904, USA. E-mail: liheng.cai@virginia.edu; Fax: +1 434-982-5660; Tel: +1 434-924-2512

b Department of Chemical Engineering, University of Virginia, 228 Wilsdorf Hall, 395 McCormick Road, Charlottesville, VA 22904, USA

c Department of Biomedical Engineering, University of Virginia, 228 Wilsdorf Hall, 395 McCormick Road, Charlottesville, VA 22904, USA

d Department of Chemistry, University of Virginia, 228 Wilsdorf Hall, 395 McCormick Road, Charlottesville, VA 22904, USA

† This article is dedicated to Dr Rubinstein on the occasion of his 70th birthday.

1. Introduction

As long as we are alive, we must breathe. This process brings bacterial, viral, and environmental particulates into our lungs. How can the lung fight against them? Biologists discovered that, in the airway, the mucus as a complex fluid traps the particulates and is cleared out from the lung by coordinated cilia beating of bronchial epithelia, reminiscent of transporting people using an escalator. The clearance of mucus is the primary innate defense mechanism that protects the lung.[1] This active transport phenomenon is ubiquitous among animals ranging from mice to giraffes despite possessing radically different airway lengths. Importantly, the impairment of this upward transport associates with mucus obstructive lung diseases;[2] these include chronic obstructive pulmonary disease (COPD), cystic fibrosis (CF), primary ciliary dyskinesia (PCD), and non-cystic fibrosis bronchiectasis.

The pathogenesis of mucus-obstructive lung diseases is multifactorial but includes a common, disease-initiating step: the generation of excessively concentrated mucus. The concentration of mucus—measured as either the wet-to-dry content of mucus or mucin concentration—has been established as a marker of mucus-obstructive lung diseases.[2,3] Under normal conditions, human airway mucus is composed of approximately 98% water, with the remaining 2% solid content consisting of 0.9% salt, 0.8% globular proteins, and 0.3% high-molecular-weight mucin biopolymers. By contrast, the solid content concentration increases to ∼5 wt% for COPD and ∼8 wt% for CF mucus.[4,5] The pathological mucus provides

an environment favorable for the formation of bacterial colonies or biofilms,[6] which further impede mucus clearance and cause chronic infection in mucus-obstructive lung diseases.[7,8] In particular, *Pseudomonas aeruginosa*, an opportunistic Gram-negative bacterium, is the dominant pathogen in late-stage diseases and is implicated in ~90% of CF related fatalities.[9–12]

The virulence and capability of *P. aeruginosa* in forming colonies or biofilms are strongly correlated to its motility,[13–15] which is determined by the interactions between bacteria and mucus.[16] The properties of mucus are largely determined by mucin biopolymers, which have a long linear peptide backbone densely grafted with many *O*-linked glycans. In the context of biochemical interactions, using mucins purified from porcine intestinal mucus and human saliva, the Ribbeck Lab discovered that mucin glycans attenuate the virulence of *P. aeruginosa* by maintaining the cell at planktonic, non-aggregate form.[17,18] In the context of biophysical interactions, the Hill Lab[19,20] found that *P. aeruginosa* are prone to form colonies in reconstituted human airway mucus with concentration matching that of the CF condition. These studies provide valuable insights into the role of bacteria-mucin/mucus interactions in the context of bacterial virulence and biofilm formation. However, reconstituted mucus or purified mucins have viscoelasticity and osmotic properties dramatically different from that in native state, as demonstrated in our previous study.[21] Consequently, it would be highly valuable to investigate the transport of bacteria through native human airway mucus.

Here, we report the transport of *P. aeruginosa* strain PA14, a human clinical isolate responsible for chronic lung infections, in normal and pathological native human airway mucus. Using our previously developed method, we harvest native human airway mucus with concentrations matching health and disease states. Furthermore, we develop a droplet-in-oil system for

quantifying the transport of individual bacterium within bulk mucus. Viscoelastic normal mucus promotes directional bacterial motility at a speed comparable to that in a low-viscosity physiological buffer. By contrast, concentrated, highly viscoelastic diseased mucus traps bacteria, reducing their motility more than 10-fold. Engineering mucus simulants with decoupled viscosity and elasticity reveals that the elasticity of complex fluids induces a shift in bacterial motility from circular to directional motion. Our discovery reveals the importance of elasticity in directional bacterial transport within complex fluids and provides insights into the biophysical mechanisms of bacterial infection in the lung.

2. Results

2.1 Droplet-in-oil system for imaging bacteria transport in native airway mucus

We use our previously developed method to harvest and concentrate native airway mucus without impairing its biophysical properties.[21,22] Specifically, we use the classic air–liquid interface (ALI) system to culture primary human bronchial epithelial (HBE) cells, which differentiate to a pseudostratified epithelium mimicking biological features *in vivo*[23–26] (Fig. 1a). Within the fully differentiated HBE cell culture, goblet cells continuously release mucins from granules to the apical chamber, where the mucin molecules swell to form a mucus hydrogel. To harvest the mucus, we add phosphate buffered saline (PBS) to the apical side of the ALI culture to swell the mucus. This allows us to collect the mucus washings without involving any chemical interventions that are known to impair mucus properties.[22] Yet, the concentration of this diluted mucus is typically ~0.1 wt% excluding salt, much lower than that of
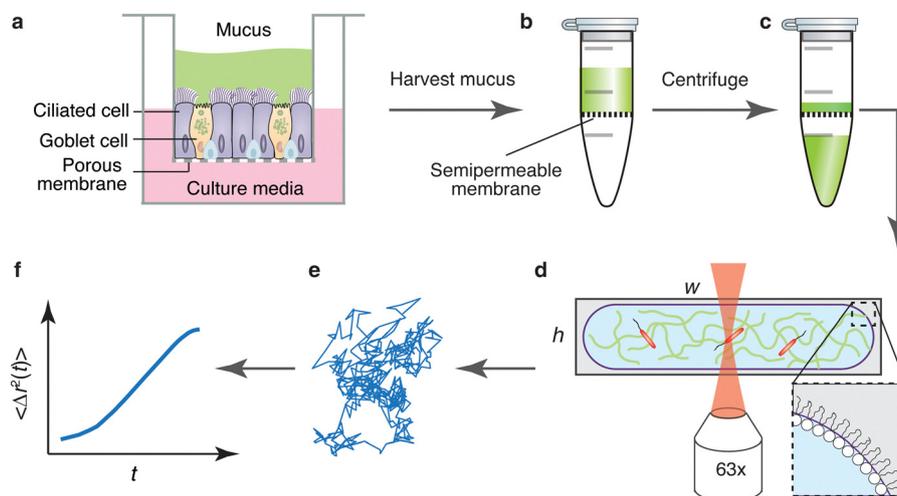

Fig. 1 The experimental set-up for quantifying the transport of *P. aeruginosa* and probe particles in native mucus and other complex fluids. (a) An air–liquid interface cell culture system is used to harvest native mucus secreted by well differentiated human bronchial epithelial cells. (b) and (c) The harvested mucus is concentrated to desired concentrations using centrifugation. The reconcentration is performed using centrifuge tubes with a semi-permeable membrane of MWCO 10 kDa. (d) A water-in-oil droplet system for quantifying the motility of probe objects in mucus using confocal microscopy (h = 0.12 mm, W = 20 mm). (e) The probe particle trajectories are then acquired from videos using particle tracking. (f) The particle motility is quantified by computing the dependence of mean-square displacement (MSD) on lag time.

mucus in health and in disease. For example, the mucus concentrations are typically of 2 wt% for health, 5 wt% for COPD, and 8 wt% CF.[4] To obtain mucus with concentrations comparable to those of physiological and pathological conditions, we reconcentrate the mucus washings using a centrifugal filter consisting of two chambers separated by a semi-permeable membrane with a molecular weight cut-off (MWCO) of 10 kDa (Fig. 1b and c). This MWCO allows water and small ions to pass through the membrane without filtering out the biopolymers in the mucus.[21,22] With this method, we harvest native mucus with desired concentrations without impairing its biophysical properties (Fig. S1).

Because of the limited amount of mucus, we develop a water-in-oil droplet system that allows for monitoring the motility of probe particles in bulk mucus of a small volume 40 μL. The system is a cylindrical glass chamber with a diameter of 20 mm and a height of 120 μm. This height is about 100 times the average size of a *P. aeruginosa*. During experiments, we focus on the cells near the center along the chamber height; this ensures that the distance from the chamber wall is more than 10 times the cell size to avoid boundary effects[27] and surface adhesion[28] on bacterial motility. To prevent unspecific interactions between the cell and the chamber surface, we pre-wet the chamber with perfluorocarbon oil, a biologically inert fluid that is widely used in droplet microfluidics for biological applications.[29] Moreover, the oil is premixed with a fluorinated surfactant molecule that can stabilize water-in-oil droplets for weeks.[30] Using this method, we create a mucus-in-oil droplet system that enables monitoring transport of particles in bulk rather than the surface of mucus, as illustrated in Fig. 1d. This capability is validated by confirming that probe particles and bacteria are nearly evenly distributed across the whole chamber height for various kinds of complex fluids (Fig. S2).

2.2 Microrheology of mucus

Using the mucus-in-oil droplet system, we perform microrheological measurements to characterize the viscoelasticity of mucus at various concentrations. The measurements involve three steps: (i) tracking the motility of individual probe particles, (ii) quantifying the mean-square-displacements (MSD), $\langle \Delta r^2(t) \rangle$, of particles, and (iii) computing the viscoelasticity of mucus using the generalized Stoke–Einstein relation,[31–33] which relates the viscoelastic spectrum $\tilde{G}(s)$ of the probed environment to the Laplace transform $\langle \Delta \tilde{r}^2(s) \rangle$ of particle MSD $\langle \Delta r^2(t) \rangle$ (Fig. 1e and f):

$$\tilde{G}(s) = \frac{2k_B T}{\pi d s \langle \Delta \tilde{r}^2(s) \rangle} \quad (1)$$

Here, k_B is the Boltzmann constant, T is the absolute temperature, d is particle diameter, and s is Laplace frequency. According to the Kramers–Kronig relations, storage modulus $G'(\omega)$ and loss modulus $G''(\omega)$ respectively correspond to the real and imaginary parts of the complex modulus $G^*(\omega)$, which is determined by substituting $i\omega$ for the Laplace frequency s in eqn (1).

Because passive microrheology relies on the thermal motion of probe particles, it is critical to prevent unspecific binding between the particles and the surrounding environment. Thus, we use polystyrene microparticles coated with poly(ethylene glycol) (PEG) polymers, a well-established approach for creating mucus inert carriers.[34,35] The particle diameter 1 μm is much larger than the correlation length of normal mucus hydrogel, $\xi \approx (k_B T/\pi)^3 \approx 20$ nm, in which $\pi \approx 500$ Pa is the osmotic pressure of 2.0 wt% normal mucus.[21,36] Such a relatively large particle avoids probing local properties of mucus, which is known to be heterogeneous and exhibits particle size dependent viscoelasticity.[37]

We record the motion of 1 μm PEGylated particles in normal mucus using high-speed fluorescence confocal microscopy at 50 frames per second (fps). Example trajectories of individual particles are shown in Fig. 2a(i). The accuracy of the particle tracking is confirmed by the overlap of the trajectories with the video for particle diffusion (Video S1). Based on the trajectory of a particle, we compute its MSD *versus* lag time $\Delta\tau$, and sample at least 200 trajectories to obtain the average MSD, as shown by the solid green line in Fig. 2b.

As mucus concentration increases, the particle motion becomes more confined, as shown by the trajectories of probe
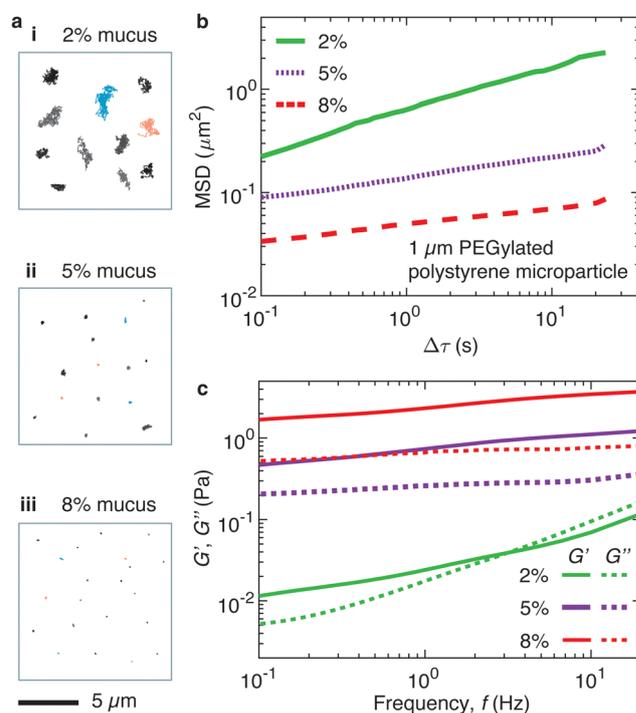
Fig. 2 Passive microrheology of native airway mucus. (a) Representative trajectories of 1 μm PEGylated polystyrene microparticles in (i) 2 wt% (normal), (ii) 5 wt% mucus (COPD), and (iii) 8 wt% (CF) mucus. For each type of mucus, more than 200 trajectories are acquired from fourteen videos for normal mucus, nine videos for COPD-like mucus, and ten videos for CF-like mucus. (b) Average mean-square-displacement (MSD) *vs.* lag time, $\Delta\tau$, of 1 μm particles in mucus of normal (green) and pathological (5%, purple dotted line; 8%, red dashed line) concentrations. (c) Storage (G') and loss (G'') modulus of mucus at various concentrations based on the MSD of 1 μm particles.

particles in COPD-like (5%) and CF-like (8%) mucus (Fig. 2a(ii) and (iii)) (Videos S2 and S3). To quantify the difference in particle diffusion, we compare the average MSD of probe particles at 30 s, the longest period that the particle trajectories can be reliably tracked before they diffuse out of the focus plane. For the 1 μm particle, the average MSD is $\sim$0.20 μm^2 and 0.09 μm^2 in COPD- and CF-like mucus, respectively; these values are an order of magnitude lower than the $\sim$2 μm^2 observed in normal mucus. We also measure the motility of 100 nm PEGylated gold nanospheres within the three mucus formulations. For these 100 nm nanospheres in the CF-like and COPD-like mucus, the average MSD is $\sim$1.0 μm^2 and $\sim$0.7 μm^2, respectively. These values are nearly one order of magnitude lower than that of $\sim$3 μm^2 observed in normal mucus (Fig. S3 and Videos S4–S6). These results highlight the heterogeneity of mucus network mesh size[37] and also suggest that the majority of mesh sizes in normal and pathological mucus are likely less than 100 nm.

We use the MSD of 1 μm probe particles to calculate the viscoelasticity of mucus (eqn (1)). At relatively low probing frequency <3 Hz or long-time scales >0.3 s, the normal mucus is more elastic with storage modulus G' greater than the loss modulus G''. Yet, at relatively high probing frequency >3 Hz, normal mucus is more of a viscous liquid with $G' < G''$ (Fig. 2c). The frequency dependent viscoelastic properties of mucus are consistent with the microrheology data using smaller PEGylated Au nanoparticles, which have a diameter 100 nm, much greater than the average mucus mesh size (Fig. S3). Importantly, at a probing frequency 14 Hz comparable to that of ciliary beating,[38] the mucus is more of a viscoelastic liquid with a loss modulus of $\sim$0.1 Pa (green lines, Fig. 2c). This behavior is consistent with the clinical observations that under coordinated ciliary beating, normal mucus behaves like a liquid that can flow out of the human airway.

Interestingly, increasing mucus concentration qualitatively changes the viscoelastic properties. The shear storage modulus of the COPD and CF mucus at the lowest probing frequency 0.1 Hz is approximately 0.4 Pa and 2 Pa, respectively (purple and red lines, Fig. 2c); these values are more than 10 times greater than that of the normal mucus, 0.01 Pa (solid green line, Fig. 2c). Importantly, the storage modulus is greater than the loss modulus across the whole frequency range explored. These results demonstrate that mucus with pathological concentrations become an elastic solid, supporting the clinical observation of impaired or failed mucus clearance in mucus-obstructive pulmonary diseases.[4] Collectively, these results indicate that native mucus exhibits viscoelasticity consistent with the understanding of mucus clearance.

2.3 Transport of *P. aeruginosa* in normal and pathological mucus

To study motility of *P. aeruginosa* in mucus, we premix the cells with mucus at prescribed concentrations, such that the average distance between two neighboring cells is at least 10 μm. This avoids communication among cells and thus allows us to focus on the behavior of a single bacterium. The *P. aeruginosa* is

genetically modified from PA14, a clinical isolate responsible for lung infection, to exhibit red fluorescent surface protein mKate2.[39] We monitor the motility of *P. aeruginosa* using high-speed fluorescence confocal microscopy. For each video, we collect a sequence of at least 1000 images at 20 fps at a Z-position at the center of the chamber and extract individual bacterium trajectories, as exemplified in Fig. 3a. For all trajectories, we overlay them with the real time movie to ensure that they accurately capture the bacterial motility. During each measurement, the bacteria are only within the mucus for less than 10 min; this short period avoids potential effects of limited nutrients within mucus on *P. aeruginosa* motility.

In the non-Newtonian, highly viscoelastic normal mucus, *P. aeruginosa* exhibits bimodal motility (Fig. 3a(ii)). Most bacteria ($\sim$82%) adopt a directional, linear motion featuring a displacement more than 50 μm, about 50 times the bacterium body size, over a period of 0.3–1 s (Video S7). By contrast, in a low viscosity, Newtonian buffer (LB medium), most bacteria exhibit circular motion, as shown by representative trajectories in Fig. 3a(i) (Video S8). A small fraction of bacteria in the normal mucus ($\sim$10%) adopt a confined, localized motion, which features a displacement less than 5 μm over 50 s (Fig. 3a(ii)). These confined bacteria are not stationary, however; they can rotate and sometimes even swim for short distances. Moreover, a bacterium can switch between these two modes. For instance, a bacterium exhibiting linear motion can get stuck and adopt the confined motion. Yet this confinement is temporary, and the bacterium can escape to resume the linear motion, as exemplified by trajectory 3 in Fig. 3a(ii). Moreover, a bacterium can exhibit an intriguing behavior where a linear swimming cell travels back adjacent to, or even along, its initial trajectory, sometimes multiple times over the course of the same path, as exemplified by trajectory 4 in Fig. 3a(ii). The confined bacteria, despite possessing intact flagellum, exhibit similar motility to the non-motile counterpart without flagellum (PA14 $\Delta fliC$) (Fig. S4 and Video S9). Note that prior studies reveal enhanced transport of rod-shaped nanoparticles (100–200 nm in length and 20–30 nm in diameter) within rat intestinal mucus compared to the spherical counterparts. Although the non-motile bacteria are rod like, their size is much greater than mucus mesh size.[40] Nevertheless, our results highlight the highly heterogeneous nature of native human airway mucus.

To further explore the difference between the *P. aeruginosa* motion in LB medium and in normal mucus, we quantify the bacterial motility by computing the MSD of each cell (Fig. 3b). To characterize the type of bacteria motion, we fit the MSD using an equation for describing two-dimensional (2D) diffusion:[41]

$$\langle r^2(\Delta\tau) \rangle = 4D_0(\Delta\tau/\tau_0)^\alpha \tag{2}$$

in which D_0 is the effective diffusivity and τ_0 is the step size or the time interval between two neighboring frames when monitoring the bacterial motility. The exponent α describes the type of diffusion: for $0 < \alpha < 1$, sub-diffusion; $\alpha = 1$, diffusion; $1 < \alpha < 2$, super-diffusion; $\alpha = 2$, ballistic motion. We fit the
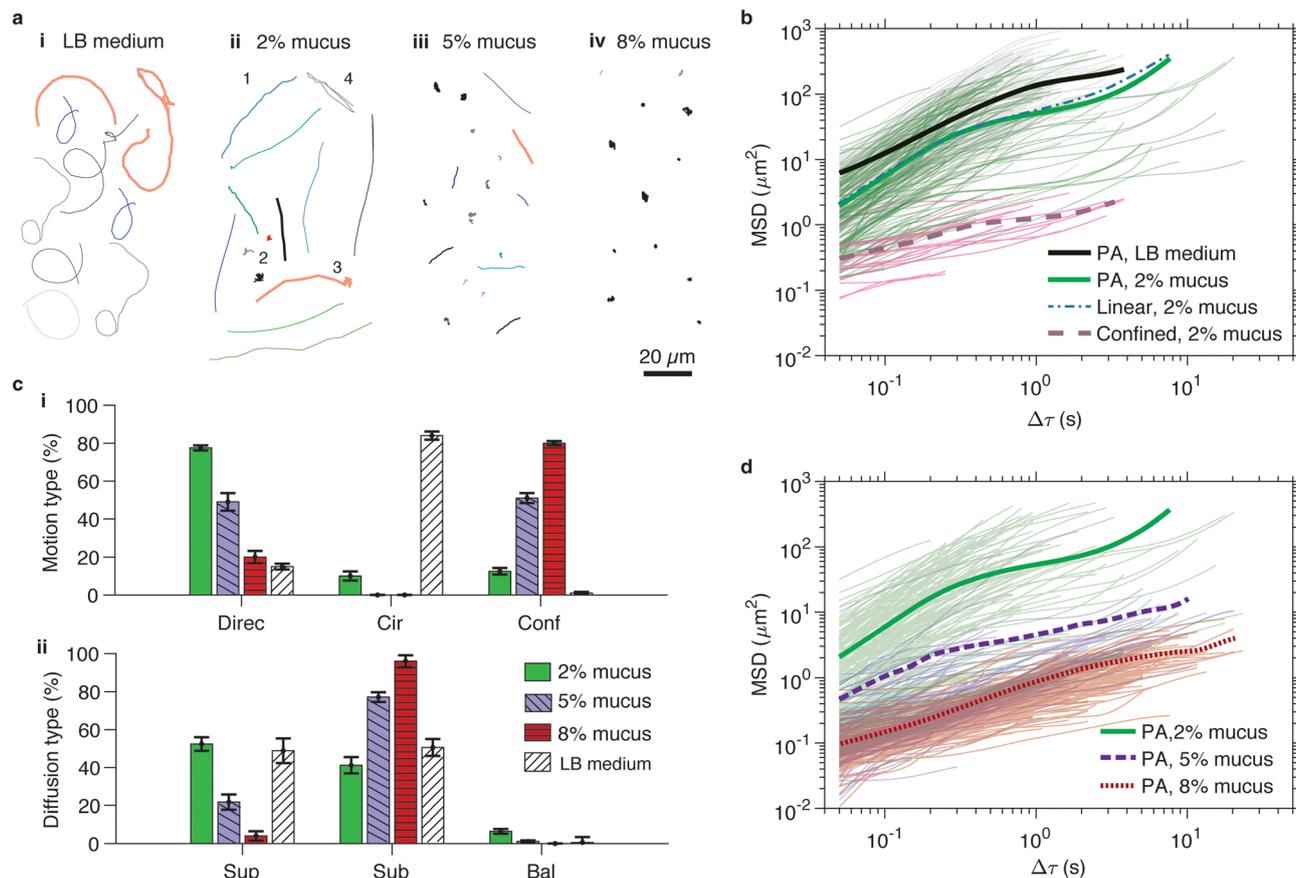
Fig. 3 Normal mucus promotes directional linear motility of *P. aeruginosa*. (a) Representative trajectories of bacteria in (i) LB medium, (ii) 2% normal mucus, (iii) 5% COPD-like mucus, and (iv) 8% CF-like mucus. We track bacteria from nine confocal microscopy videos for 2% mucus, eight videos for 5% mucus, eleven videos for 8% mucus, and five videos for LB medium. (b) Dependence of mean-square displacement (MSD) on lag time $\Delta\tau$ for bacteria in normal mucus (green) and LB medium (black). Thin solid lines: MSD of individual bacteria; thick solid lines: averaged MSD over 200 trajectories. Dotted and dashed lines represented the averaged MSD of linear (blue) and confined (purple) *P. aeruginosa* trajectories, respectively. (c) Fractions of the types of (i) motion and (ii) diffusion of bacteria in LB medium and mucus with normal and pathological concentrations. Data are presented as mean ± standard deviation for n = 3–5, where n is the number of mucus batches. (d) MSD of bacteria in mucus of different concentrations. The value of α is determined by using $\langle r^2(\Delta\tau) \rangle = 4D_0(\Delta\tau/\tau_0)^\alpha$ to fit the MSD curves up to 1.5 s: super diffusion ($1 < \alpha < 2$), sub diffusion ($\alpha < 1$), and ballistic motion ($\alpha = 2$).

data up to 1.5 s, below which the MSD curves exhibit a power law dependence on the lag time, such that the values of D_0 and α can be reliably determined, as shown by the thin solid lines in Fig. 3b. Further, we define confined trajectories as those associated with bacteria moving with a distance less than its own body size (~1.0 μm) within one second, $\langle r^2(\Delta\tau) \rangle|_{\Delta\tau=1s} < 1$ μm^2.

Despite marked differences in motion type, the average displacement of *P. aeruginosa* exhibiting directional motion in normal mucus is comparable to that in LB medium, as shown by the adjacent average MSD curves (thick solid lines in Fig. 3b). To further quantify the difference between *P. aeruginosa* motility in LB and normal mucus, we compare the correlation between effective diffusion coefficient D_0 to motion type exponent α for each bacterium, as shown in Fig. S5. For confined bacteria in normal mucus, the average D_0 (0.22 ± 0.01 μm^2) is more than one order of magnitude lower than that in LB buffer (5.40 ± 0.27 μm^2). However, the fraction of confined bacteria is relatively small (18%), much lower than that with directional linear motion (82%) (green bars, Fig. 3c(i)).

Consequently, there is no statistically significant difference in average D_0 for all cells, as well as for any cells that only exhibit directional motion, as shown by the nearly overlapped thick dashed green line and thick green line in Fig. 3b. Consistent with these observations, for all *P. aeruginosa* in normal mucus (directional and confined), the average D_0 is 2.40 ± 0.29 μm^2 and 58% of cells are super-diffusive ($\alpha > 1$) (left green bar, Fig. 3c(ii)). For *P. aeruginosa* exhibiting only directional motion, the average D_0 is 4.10 ± 0.15 μm^2. These values are comparable to bacteria in LB buffer, which have an average D_0 of 5.40 ± 0.27 μm^2 and 56% cells are super-diffusive. Yet, the average value of α for bacteria in normal mucus is 1.29, higher than 1.04 for cell in LB buffer; this difference further reflects the tendency of *P. aeruginosa* to adopt linear motion over circular motion in normal mucus. These results show that normal mucus promotes linear directional motion of *P. aeruginosa* to enable fast transport.

Increasing the mucus concentrations to pathological values dramatically slows the transport of *P. aeruginosa*, as shown by example trajectories in COPD-like 5% mucus and CF-like 8%

mucus (Fig. 3a(iii) and (iv), Videos S10, S11). Compared to *P. aeruginosa* in normal mucus, in COPD-like mucus, the fraction of bacteria exhibiting directional transport is dramatically lower (44%) and the fraction of confined cells is significantly higher (56%). Rarely do some bacteria displace more than 50 μm, which can be easily achieved by bacteria in normal mucus. Yet the bacteria often can move by a distance ~ 20 μm, about 20 times that of the bacterium body size (purple lines, Fig. 3d). By contrast, in CF-like mucus, 82% cells are confined, and few can move > 10 μm (light red lines in Fig. 3d, red bars in Fig. 3c(i)). Consistent with this observation, nearly all bacteria (96%) exhibit sub-diffusive motion (red bars, Fig. 3c(ii)). Quantitatively, the average effective diffusion coefficient D_0 is 0.10 ± 0.09 μm^2 in CF-like mucus, nearly two and a half times lower than that in COPD-like mucus, 0.23 ± 0.16 μm^2 (Fig. S6).

2.4 Elasticity is critical to directional *P. aeruginosa* transport in complex fluids

Our experimental results show that in a low viscosity, Newtonian buffer, *P. aeruginosa* exhibits mainly circular motion. By contrast, in a highly viscoelastic, non-Newtonian normal airway mucus, *P. aeruginosa* mainly exhibit directional motion, with an average transport speed comparable to that in LB buffer. In highly concentrated, elastic pathological mucus, the bacteria are mainly confined. Based on these results, we hypothesize that elasticity (storage modulus) is critical to efficient transport of *P. aeruginosa* in complex fluids.

To test this hypothesis, we seek to engineer mucus simulants with similar viscosity (or viscous modulus) but various elasticity (or elastic modulus). Historically, achieving this has been challenging due to the complex nature of mucus as a biological hydrogel. However, previous studies, including our own, suggest that the intricate viscoelasticity of mucus arise primarily from three essential molecular features: (i) entanglements formed by large molecular weight (MW) gel-forming mucins, (ii) reversible associations formed by the hydrophobic domains of mucins, and (iii) a relatively large mass fraction of (~ 30 wt%) small low MW proteins and molecules within the solid content (excluding salt) of mucus. Instead of using solutions composed of a single polymer species, we use a hybrid polymer solution consisting of low MW alginate and high MW PEO polymers[42] as mucus simulants. The low MW alginate allows for tuning viscosity, whereas the high MW PEO can form entanglements, which are known to be responsible for the elasticity of polymer solutions.[43] Moreover, the ether oxide groups of PEO and the hydroxyl groups of alginate can form hydrogen bonding,[44] a kind of reversible associations that allow for enhanced viscosity at relatively low concentrations. This approach enables the creation of mucus simulants by mimicking the three essential molecular features of mucus.

We denote a mucus simulant as Alg^{x}PEO^y_z, in which x and y are the concentration (wt/vol%) of alginate and PEO, respectively, and z is the MW of the PEO in g mol^{-1}. Since it is relatively easy to obtain large sample volumes, we use bulk rheology as the primary method to characterize the viscoelasticity of mucus simulants. In contrast, we rely on microrheology

to characterize native mucus for two reasons. First, it is difficult to collect enough native mucus for bulk rheology. Second, recent studies suggest that bulk rheological measurements of mucus are strongly influenced by the mucus–air interface.[45] Nevertheless, using a mucus simulant as an example, we confirm that both bulk rheology and microrheology yield consistent measurements in viscoelastic properties (Fig. S7).

By tuning the concentration and MW of these two polymers, we create four kinds of mucus simulants, all of which have a viscous modulus at the lowest frequency (0.1 rad s^{-1}) on the order of 10 mPa (empty symbols, Fig. 4a), comparable to that of normal mucus (dashed lines, Fig. 2c). Importantly, for all mucus simulants, the viscous modulus is nearly the same over a wide range of frequency (0.1 to 100 rad s^{-1}), as shown by the nearly overlapping empty symbols in Fig. 4a. By contrast, the elastic modulus varies in a wide range from ~ 2 mPa to 100 mPa at 0.1 rad s^{-1}, as shown by the filled symbols on the left of the Fig. 4a. Specifically, the first simulant, a highly viscous liquid, Alg$^{0.5}$PEO$^{0.4}_{1M}$, exhibits G' more than 10 times lower than G'' at all probing frequencies, with moduli increasing in a similar manner with frequency *via* a power law (triangles, Fig. 4a). The second simulant, an elastic fluid mimicking CF-like mucus, Alg$^{0.8}$PEO$^{0.29}_{1M}$, exhibits G' greater than G'' over the entire frequency range (0.1–100 rad s^{-1}) (squares, Fig. 4a). The remaining two simulants, mimicking normal mucus, Alg$^{1.0}$PEO$^{0.5}_{300k}$ and Alg$^{0.5}$PEO$^{1.1}_{100k}$, have different compositions but exhibit nearly identical viscoelastic behavior (circles and diamonds, Fig. 4a). Note that the Alg–PEO system is not a gel or near gel point as there are no crosslinks. Instead, it is simply a mixture of two polymers in buffer. The system is not a perfect replacement for mucus rheology but allows for dissecting roles of elastic and viscous moduli in bacteria transport in complex fluids.

In the mucus simulant with the lowest elasticity (Alg$^{0.5}$PEO$^{0.4}_{1M}$), the bacteria primarily exhibits rapid circular motion, as shown by the representative trajectories in Fig. 4b(i) and Video S12; this behavior is similar to that observed in low viscosity, Newtonian LB buffer (Fig. 3a(i)). As expected, in the highly elastic mucus simulant (Alg$^{0.8}$PEO$^{0.29}_{1M}$), most bacteria are confined locally, with a displacement less than twice the bacterium's body size (2 μm) within the field of view (Fig. 4b(iv)), as shown by Video S13. These differences are further confirmed by the more than 10-fold difference in the average MSD of *P. aeruginosa*, as indicated by the thick red and black lines in Fig. 4c.

In the mucus simulant with intermediate elasticity (Alg$^{1.0}$PEO$^{0.5}_{300k}$), *P. aeruginosa* primarily exhibits linear, directional motion (Fig. 4b(ii)), as shown in Video S14. Interestingly, in another mucus simulant (Alg$^{0.5}$PEO$^{1.1}_{100k}$) with a different polymer composition but nearly the same intermediate elasticity, most bacteria exhibit linear, directional motion (Fig. 4b(iii) and Video S15). Quantitatively, the average MSD for the bacteria in these two mucus simulants is nearly identical, as shown by the thick green and blue lines in Fig. 4c. These results demonstrate that the bacteria transport is determined by the flow properties, rather than the composition of the complex fluids, and that elasticity plays a critical role in facilitating the directional transport of *P. aeruginosa*.
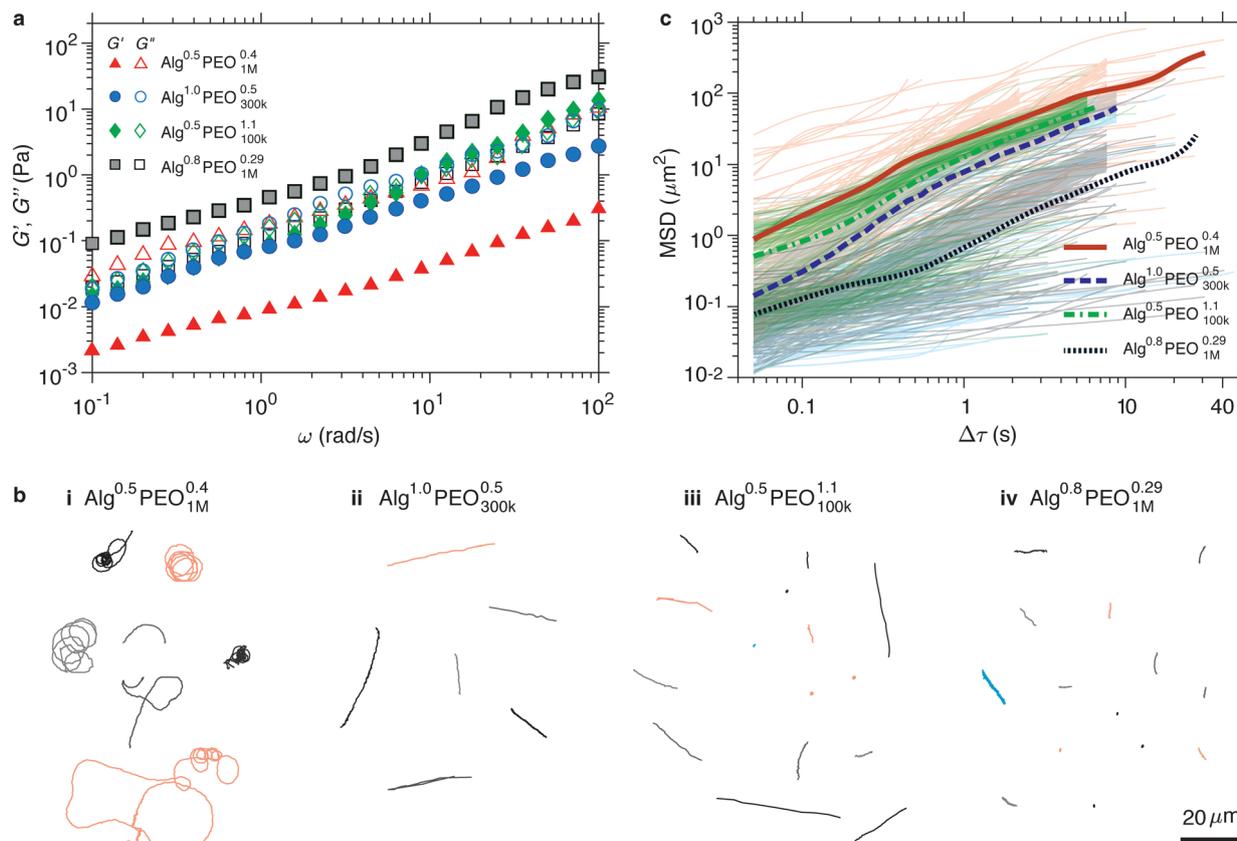
Fig. 4 Elasticity is critical to directional transport of *P. aeruginosa* in complex fluids. (a) Storage and loss moduli of mucus simulants with nearly the same loss modulus but different storage modulus. The mucus simulants are made by two polymers, alginate and polyethylene oxide (PEO): $Alg^xPEO^y_z$, in which x and y are, respectively, the concentration of alginate and PEO in % (wt/vol), and z denotes the MW of the PEO in g mol^{-1}. (b) Representative trajectories for bacteria in each of the mucus simulants: (i) $Alg^{0.5}PEO^{0.4}_{1M}$, (ii) $Alg^{1.0}PEO^{0.5}_{300k}$, (iii) $Alg^{0.5}PEO^{1.1}_{100k}$, and (iv) $Alg^{0.8}PEO^{0.29}_{1M}$. We tracked four confocal microscopy videos for $Alg^{0.5}PEO^{0.4}_{1M}$, six videos for $Alg^{1.0}PEO^{0.5}_{300k}$, five videos for $Alg^{0.5}PEO^{1.1}_{100k}$, and seven videos for $Alg^{0.8}PEO^{0.29}_{1M}$. More elastic mucus simulants promote directional linear motility of bacteria but traps the bacteria when it becomes highly elastic. (c) Average MSD of PA14 in mucus simulants. Each average (thick solid lines) is based on at least 200 trajectories (thin lines).

2.5 Higher viscosity induces *P. aeruginosa* confinement but does not change motion type

Next, we explore the roles of viscosity in the transport of *P. aeruginosa* in complex fluids. By tuning the concentration and MW of alginate and PEO, we create three mucus simulants, all of which have a storage modulus at the lowest frequency (0.1 rad s^{-1}) of approximately 30 mPa (filled symbols, Fig. 5a), comparable to that of normal mucus (solid lines, Fig. 2e). Importantly, for all mucus simulants, the elastic modulus exhibits nearly the same frequency dependent behavior over the entire frequency range (0.1 to 100 rad s^{-1}) (empty symbols in Fig. 5a). By contrast, the viscous modulus varies widely, ranging from $\sim$15 mPa to 300 mPa at 0.1 rad s^{-1}, as shown by the empty symbols on the left of Fig. 5a. Specifically, the mucus simulants can be categorized into three groups: (1) a highly viscous liquid, $Alg^{1.5}PEO^3_{300k}$, where G' is more than 10 times lower than G'' (with $G''/G' \sim 10$, diamonds, Fig. 5a); (2) a liquid with intermediate viscosity, $Alg^{1.0}PEO^{2.5}_{100k}$, where the G'' is slightly greater (3–5 times) than G' over the entire frequency range (triangles, Fig. 5a); and (3) a low viscosity liquid, $Alg^{0.5}PEO^{1.1}_{100k}$, where G'' is comparable to G' at relatively high

frequencies ($>$1 rad s^{-1}) but becomes lower than the G' at low frequencies (circles, Fig. 5a).

We find that bacteria exhibit no circular motion regardless of viscosity, but their transport speed decreases dramatically in mucus simulants with higher viscosity (Fig. 5b). Specifically, in the simulant with the highest viscosity ($Alg^{1.5}PEO^3_{300k}$), the bacteria are locally confined (Fig. 5b(iii) and Video S16), with an MSD less than 1 μm^2 within 50 s (thick green line, Fig. 5c). In the simulant with intermediate viscosity ($Alg^{1.0}PEO^{2.5}_{100k}$), most bacteria exhibit long-range, directional motion, while $\sim$20% bacteria remain confined (Fig. 5b(ii) and Video S17). This bimodal motility is similar to that observed in both normal and pathological mucus (Fig. 3a(ii)–(iv)). However, the bacteria only move by their body size with an MSD of $\sim$1 μm^2 within 1 s, much less than that in normal mucus (MSD $\sim$ 50 μm^2 at 1 s). By contrast, in the mucus simulant with the lowest viscosity ($Alg^{0.5}PEO^{1.1}_{100k}$), the bacteria exhibit markedly faster directional transport, with an MSD of 10 μm^2 within 1 s (Fig. 5b(i) and Video S15). These results indicate that higher viscosity slows down bacterial transport speed but does not alter the type of motion (Fig. S8). Collectively, our findings
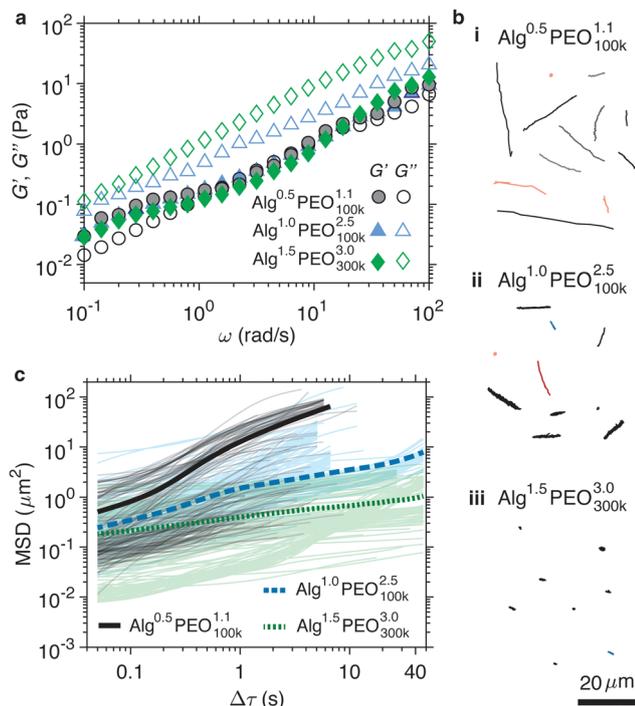
Fig. 5 Higher viscosity induces confinement of bacteria but does not alter their motion type. (a) Mucus simulants with nearly the same storage modulus but different loss modulus. (b) Representative trajectories for *P. aeruginosa* in the mucus simulants: (i) $Alg^{0.5}PEO^{1.1}_{100k}$, (ii) $Alg^{1.0}PEO^{2.5}_{100k}$, and (iii) $Alg^{1.5}PEO^{3.0}_{300k}$. More viscous simulants reduce PA14 motility towards confinement, but do not induce changes in motion type. (c) MSD of bacteria in mucus simulants. Thick lines represent the average MSD based on at least 200 trajectories (thin lines).

suggest that the motion type of *P. aeruginosa* is primarily determined by the elasticity of complex fluids, rather than their viscosity.

3. Discussion and conclusion

Bacteria living in mucus have formed an evolutionary partnership with us to enable robust mucosal defense. When forming colonies, however, they are also the cause of infection and disease. Existing studies largely rely on reconstituted mucus,[19] purified mucins,[46] or commercially available mucins,[47] which we demonstrated have properties dramatically different from that in a native state.[21] This is largely because mucus is a very delicate biological hydrogel with properties sensitive to biochemical treatments and aggressive processing. The biophysical properties such as viscoelasticity and osmotic pressure of human airway mucus are determined by two secreted gel-forming mucins, MUC5B and MUC5AC. The gel-forming mucins interweave *via* physical entanglements and hydrophobic associations among globular domains. These associations can dissociate upon mechanical shear imposed by cilia beating, such that mucus can flow like a liquid during mucus clearance. Moreover, the associations can be altered by chemical reagents such as surfactants, as well as by pH,[48] leading to the change of mucus viscoelasticity and biophysical properties. For instance,

typical studies of mucins are performed after extraction and purification, which involve using highly denaturing solvents (*e.g.*, 6-M guanidinium chloride) to solubilize mucus;[49] this process transforms native mucus from a viscoelastic gel to a low viscosity liquid. Additionally, our previous studies[21] showed that the osmotic pressure of reconstituted human airway mucus, measured using a membrane osmometer, decreases markedly with the increase of the MWCO of the semipermeable membrane. By contrast, regardless of concentration, native human airway mucus exhibits an osmotic pressure nearly independent of the membrane MWCO (Fig. S9). Such a marked difference in both viscoelasticity and osmotic pressure indicates that it is essential to maintain mucus at its native state.

In the context of mucus clearance, the observed increase in mucus elasticity at pathological concentrations (Fig. 2c) is consistent with recent biological discoveries and clinical observations. We previously discovered that cilia are beating in a frictionless gel[21] rather than a conventionally thought low viscosity liquid.[50] The gel is formed by membrane-spanning mucin-type glycoproteins[51] and large, linear mucopolysaccharides[52] densely grafted onto cilia, structurally reminiscent of the bottlebrush for cleaning lab glassware but on a molecular scale. This mucus gel-on-brush model unifies the pathogeneses of mucus obstructive lung diseases, in which concentrated mucus generates an osmotic pressure that depletes water from the brush-like gel and thus physically collapses cilia.[21] Moreover, by sampling nearly 1000 patients, subsequent clinical studies confirmed that mucus osmotic pressure is a biophysical marker of chronic bronchitis.[3] In addition to elevated osmotic pressure, increased mucus elasticity may further impair mucus clearance, which requires mucus to flow like a liquid. The combination of the collapse of cilia and increased mucus elasticity results in mucus stasis, which is a hallmark of mucus obstructive lung diseases.

The dramatic difference between bacterial motility in normal and pathological mucus highlights the important roles of mucus in the formation of bacterial colonies. In normal mucus, *P. aeruginosa* are not confined but exhibit a rapid motion, with an average swimming speed 43.1 ± 1.4 μm s^{-1} comparable to that 44.5 ± 1.0 μm s^{-1} in LB medium. This behavior is somewhat consistent with previous findings that mucin biopolymers tend to promote the surface motility of *P. aeruginosa*, preventing the formation of biofilms.[53,54] By contrast, in pathological mucus, *P. aeruginosa* are trapped and exhibit minimum displacement. This behavior is reminiscent of classical biofilm formation process, in which bacteria switch lifestyle from swarming to nonmotile upon adhering to a solid substrate.[55] Yet, the major difference is that there is no solid substrate within the mucus gel. Thus, one possible explanation is that bacteria are physically trapped by the tight mesh of highly elastic pathological mucus hydrogel. Another possible explanation is that pathological mucus suppresses the expression of genes-encoded proteins, including *fliC* that encodes flagellin, involved in flagellum-mediated motility.[56] Note that although the shut-off of flagellin is rapid, with 80% reduction of *fliC*

mRNA within 2 hours of exposure to sputum from CF patients,[56] this time scale is much longer than that in our experiments (< 30 min). Moreover, *P. aeruginosa* may sense the extent of surface stiffness *via* retraction of type IV pili,[57] which are important for *P. aeruginosa* virulence through type IV pili-mediated virulence pathways.[58,59] It would be interesting to determine whether trapping *P. aeruginosa* within mucus hydrogel triggers the change of bacteria phenotype[55] and induces the expression of virulence genes.[60]

An intriguing observation is that as a single flagellum bacterium, *P. aeruginosa* exhibits circular motion in a low viscosity, Newtonian LB buffer. This circular motion occurs in bulk liquid. By contrast, classical understanding is that bacteria swim in clockwise circular motion near a solid boundary.[61] When a singly flagellated bacterium swims in a viscous liquid, its helical flagellum rotates. Simultaneously, to balance the torque generated by the flagellum rotation, the cell body rotates in the opposite direction. Near a solid surface, however, the viscous liquid closer to the boundary exerts more hydrodynamic drag on a moving object than the one further away. Thus, both the rotating cell body and flagellum experience a non-zero net lateral drag force near the solid boundary but along opposite directions. This generates a non-zero net torque that constantly alters the direction of bacterial swimming, resulting in circular motion of bacteria near an interface. The boundary effects on bacterial motion become amplified at small bacteria-substrate distance (< 200 nm)[56] but diminish as the distance is greater than 10 μm,[62] approximately 10 times of bacterial body length. In our experiments, the bacteria-substrate distance is ∼50 μm (Fig. S2), and we have confirmed the circular motion through multiple independent measurements. Moreover, the unexpected circular motion occurs not only in the LB buffer but also in a highly viscous mucus simulant ($Alg^{0.5}PEO^{0.4}_{1M}$) (Fig. 4b(i)); this mucus simulant has a complex viscosity more than 40 times of water and exhibits G' more than 10 times lower than G'' across the entire probing frequency range from 0.1 to 100 rad s^{-1} (triangles, Fig. 4a). The difference is that the average diameter of the circular trajectories is 8.6 ± 0.4 μm in the mucus simulant (Fig. S10a); this value is significantly lower than 17.9 ± 0.5 μm in LB medium (Fig. S10b). Moreover, the observed diameter in the bulk LB medium is slightly lower than the lower end for the distribution of diameter for *E. coli* near interfaces (20–100 μm).[61–64] Since single-flagellated bacterium can turn by exploiting bulking of its hook connecting the flagellum filament and the cell body,[65] quantifying the axis misalignment between flagellum and cell body might provide insights into the mechanism of circular motion. Nevertheless, our findings lead to an open question on the mechanisms of circular motion of single-flagellated bacterium in bulk viscous liquids.

The most interesting, perhaps striking, finding is that elasticity promotes the directional, linear motion of *P. aeruginosa* in highly viscoelastic normal mucus and complex fluids. This conclusion is based on manually counting all bacterial trajectories, as no reliable algorithm exists to automatically classify transport modes. An alternative approach to assess directionality is to introduce a "straightness" parameter, defined as the ratio of end-to-end displacement to the total path length or the sum of each step between frames. A value approaching 1 indicates highly directional motion. Although this metric may underestimate the fraction of linear trajectories (*e.g.*, back-and-forth linear motion and half circles), the results are qualitatively consistent with manual counts (Fig. S11 and S12).

Although it has yet to be elucidated the biological mechanism of elasticity-enhanced bacterial motility, our discovery has far-reaching implications in bacterial motility in complex fluids. Decades of research have demonstrated that viscoelasticity plays a critical role in bacterial motility in complex fluids.[66–69] For instance, it was found that *Helicobacter pylori*, a bacterium that lives in stomach mucus, produces chemicals to elevate the pH of mucin gel; this reduces the viscosity of its local environment and, therefore, allows bacterial motility in porcine gastric mucin solutions.[70] In synthetic high MW polymer solutions, by measuring the average speed of flagellated bacterial species including *P. aeruginosa*, it was found that bacteria exhibit maximum swimming velocity in solutions of ∼2 mPa s (about twice of water viscosity) and becomes immobilized in solution of high viscosity (> 60 mPa s). However, this widely accepted view was challenged by a recent study, which shows that there is no such non-monotonic dependence of bacteria motility on solution viscosity.[66] It was proposed that motion of flagellated bacteria is primary due to the fast-rotating flagella, which experience a lower viscosity than the cell body because of local shear-thinning of polymer solutions.[66] In colloidal suspensions, the hydrodynamic interaction between individual bacterium and the suspended microparticles reduces bacterial wobbling, which in turn enhances bacteria motility.[71] Nevertheless, in these complex fluids, the viscous and elastic moduli are intrinsically coupled. By contrast, our mucus simulants are composed of low and high MW linear polymers that can form reversible hydrogen bonds, enabling truly decoupled viscous and elastic moduli. These mucus simulants may provide a model system for probing the challenging physics of bacterial motility in non-Newtonian fluids.

In summary, we have studied the motility of *P. aeruginosa* in normal and pathological native human airway mucus. In the non-Newtonian, highly viscoelastic normal mucus, the bacteria primarily exhibit a directional, linear motion with a speed comparable to that in a Newtonian, low-viscosity physiological buffer. By contrast, elastic, concentrated pathological mucus traps bacteria, reducing their motility by more than 10-fold. By engineering mucus simulants with decoupled viscosity and elasticity, we discover that elasticity, rather than viscosity, determines the type of bacterial transport. Slightly more elastic fluids induce a transition in bacterial motility from primarily circular, non-directional to linear, directional motion. By contrast, increasing viscosity slows bacterial transport speed but does not change their motion type. We note that our studies are restricted to the transport of individual bacterium in 2D space. Resolving detailed motion of flagellum[72,73] and cell body in three-dimensional (3D) space[74–76] may provide additional

insights into bacterial transport in mucus. Additionally, our mucus simulants are composed of simple linear polymers. However, mucins are a kind of bottlebrush biopolymer, featuring a large polypeptide backbone that is heavily glycosylated with many sugar chains.[51,77,78] It would be interesting to use bottlebrush polymer solutions as mucus simulants to explore the roles of bottlebrush molecular architecture on bacteria transport.[79–81] In the context of clinical relevance, it would be important to explore how bacteria/mucus as a composite gel impacts the efficiency of mucociliary clearance.[21,82,83] In the context of soft matter physics, bacteria as an active matter often exhibit emergent behavior as a collective.[84–89] It would be worthwhile to explore the roles of elastic modulus on the collective behavior of bacteria in complex fluids. Nevertheless, our results collectively show that elasticity promotes directional transport of *P. aeruginosa* in native human airway mucus and complex fluids. This discovery not only provides new insights into the roles of mucus in bacterial infection and mucosal defense but also opens new research directions in active matter in complex fluids.[74,89–91]

Author contributions

LHC conceived and supervised the whole study. RD performed the experiments. ZJH helped with HBE cell culture and mucus harvesting. RD and LHC analyzed the data. LHC and RD prepared the figures. LHC and RD wrote the paper.

Conflicts of interest

The authors declare no competing interests.

Data availability

All data are available in the manuscript or the supplementary information (SI). Supplementary information: materials and methods, Fig. S1–S12 and Videos S1–S17. See DOI: https://doi.org/10.1039/d5sm00659g.

Acknowledgements

References

1 J. V. Fahy and B. F. Dickey, *N. Engl. J. Med.*, 2010, **363**, 2233–2247.

2 R. C. Boucher, *N. Engl. J. Med.*, 2019, **380**, 1941–1953.

3 M. Kesimer, A. A. Ford, A. Ceppe, G. Radicioni, R. Cao, C. W. Davis, C. M. Doerschuk, N. E. Alexis, W. H. Anderson, A. G. Henderson, R. G. Barr, E. R. Bleecker, S. A. Christenson, C. B. Cooper, M. K. Han, N. N. Hansel, A. T. Hastie, E. A. Hoffman, R. E. Kanner, F. Martinez, R. Paine, P. G. Woodruff, W. K. O'Neal and R. C. Boucher, *N. Engl. J. Med.*, 2017, **377**, 911–922.

4 D. B. Hill, P. A. Vasquez, J. Mellnik, S. A. McKinley, A. Vose, F. Mu, A. G. Henderson, S. H. Donaldson, N. E. Alexis, R. C. Boucher and M. G. Forest, *PLoS One*, 2014, **9**, 1–11.

5 D. B. Hill, B. Button, M. Rubinstein and R. C. Boucher, *Physiol. Rev.*, 2022, **102**, 1757–1836.

6 S. Sethi, J. Maloney, L. Grove, C. Wrona and C. S. Berenson, *Am. J. Respir. Crit. Care Med.*, 2006, **173**, 991–998.

7 J. J. Smith, S. M. Travis, E. P. Greenberg and M. I. Welsh, *Cell*, 1996, **85**, 229–236.

8 D. J. Evans, P. S. Matsumoto, J. H. Widdicombe, C. Li-Yun, A. A. Maminishkis and S. S. Miller, *Am. J. Physiol.: Cell Physiol.*, 1998, **275**, C1284–C1290.

9 K. Botzenhardt and G. Doring, *Ecology and epidemiology of Pseudomonas aeruginosa*, 1993.

10 N. Cramer, J. Klockgether, K. Wrasman, M. Schmidt, C. F. Davenport and B. Tümmler, *Environ. Microbiol.*, 2011, **13**, 1690–1704.

11 M. M. Rowe, steven; M.D., Stacey Miller, B.S., and Eric J. Sorscher, *N. Engl. J. Med.*, 2015, **352**, 1992–2001.

12 R. L. Gibson, J. L. Burns and B. W. Ramsey, *Am. J. Respir. Crit. Care Med.*, 2003, **168**, 918–951.

13 D. Drake and T. C. Montie, *J. Gen. Microbiol.*, 1988, **134**, 43–52.

14 G. A. O'Toole and R. Kolter, *Mol. Microbiol.*, 1998, **30**, 295–304.

15 B. I. Kazmierczak, M. Schniederberend and R. Jain, *Curr. Opin. Microbiol.*, 2015, **28**, 78–82.

16 M. Zanin, P. Baviskar, R. Webster and R. Webby, *Cell Host Microbe*, 2016, **19**, 159–168.

17 J. Y. Co, G. Cárcamo-Oyarce, N. Billings, K. M. Wheeler, S. C. Grindy, N. Holten-Andersen and K. Ribbeck, *npj Biofilms Microbiomes*, 2018, **4**, 1–8.

18 K. M. Wheeler, G. Cárcamo-Oyarce, B. S. Turner, S. Dellos-Nolan, J. Y. Co, S. Lehoux, R. D. Cummings, D. J. Wozniak and K. Ribbeck, *Nat. Microbiol.*, 2019, **4**, 2146–2154.

19 H. Matsui, V. E. Wagner, D. B. Hill, U. E. Schwab, T. D. Rogers, B. Button, R. M. Taylor, R. Superfine, M. Rubinstein, B. H. Iglewski and R. C. Boucher, *Proc. Natl. Acad. Sci. U. S. A.*, 2006, **103**, 18131–18136.

20 K. R. Rouillard, W. J. Kissner, M. R. Markovetz and D. B. Hill, *mSphere*, 2022, 7, e00291-22.

21 B. Button, L.-H. Cai, C. Ehre, M. Kesimer, D. B. Hill, J. K. Sheehan, R. C. Boucher and M. Rubinstein, *Science*, 2012, **337**, 937–941.

22 L.-H. Cai, The University of North Carolina at Chapel Hill, 2012.

23 M. L. Fulcher, S. Gabriel, K. A. Burns, J. R. Yankaskas and S. H. Randell, *Methods Mol. Med.*, 2005, **107**, 183–206.

24 R. Wu, G. H. Sato and M. J. Whitcutt, *Toxicol. Sci.*, 1986, **6**, 580–590.

25 Z. J. He, C. Chu, R. Dickson, K. Okuda and L. H. Cai, *Am. J. Physiol.: Lung Cell. Mol. Physiol.*, 2024, **326**, L292–L302.

26 A. A. Pezzulo, T. D. Starner, T. E. Scheetz, G. L. Traver, A. E. Tilley, B. G. Harvey, R. G. Crystal, P. B. McCray and J. Zabner, *Am. J. Physiol.: Lung Cell. Mol. Physiol.*, 2011, **300**, 25–31.

27 I. Jurado-Martín, M. Sainz-Mejías and S. McClean, *Int. J. Mol. Sci.*, 2021, **22**, 3128.

28 J. Bell, S. Johnson, B. Pugnet and J. X. Tang, *Biophys. J.*, 2025, **124**, 1693–1703.

29 M. T. Guo, A. Rotem, J. A. Heyman and D. A. Weitz, *Lab Chip*, 2012, **12**, 2146–2155.

30 C. Holtze, A. C. Rowat, J. J. Agresti, J. B. Hutchison, F. E. Angilè, C. H. J. Schmitz, S. Köster, H. Duan, K. J. Humphry, R. A. Scanga, J. S. Johnson, D. Pisignano and D. A. Weitz, *Lab Chip*, 2008, **8**, 1632–1639.

31 T. G. Mason, *Rheol. Acta*, 2000, **39**, 371–378.

32 L.-H. H. Cai, S. Panyukov and M. Rubinstein, *Macromolecules*, 2011, **44**, 7853–7863.

33 T. Mason and D. Weitz, *Phys. Rev. Lett.*, 1995, **74**, 1250–1253.

34 J. T. Huckaby and S. K. Lai, *Adv. Drug Delivery Rev.*, 2018, **124**, 125–139.

35 J. Suh, K.-L. Choy, S. K. Lai, J. S. Suk, B. C. Tang, S. Prabhu and J. Hanes, *Int. J. Nanomed.*, 2007, **2**, 735–741.

36 R. Tarran, *Proc. Am. Thorac. Soc.*, 2004, **1**, 42–46.

37 S. K. Lai, Y.-Y. Wang, D. Wirtz and J. Hanes, *Adv. Drug Delivery Rev.*, 2009, **61**, 86–100.

38 J. Yager, T. M. Chen and M. J. Dulfano, *Chest*, 1978, **73**, 627–633.

39 D. Shcherbo, C. S. Murphy, G. V. Ermakova, E. A. Solovieva, T. V. Chepurnykh, A. S. Shcheglov, V. V. Verkhusha, V. Z. Pletnev, K. L. Hazelwood, P. M. Roche, S. Lukyanov, A. G. Zaraisky, M. W. Davidson and D. M. Chudakov, *Biochem. J.*, 2009, **418**, 567–574.

40 M. Yu, J. Wang, Y. Yang, C. Zhu, Q. Su, S. Guo, J. Sun, Y. Gan, X. Shi and H. Gao, *Nano Lett.*, 2016, **16**, 7176–7182.

41 S. S. Olmsted, J. L. Padgett, A. I. Yudin, K. J. Whaley, T. R. Moench and R. A. Cone, *Biophys. J.*, 2001, **81**, 1930–1937.

42 J. Zhu, Y. He, L. Kong, Z. He, K. Y. Kang, S. P. Grady, L. Q. Nguyen, D. Chen, Y. Wang, J. Oberholzer and L. H. Cai, *Adv. Funct. Mater.*, 2022, **32**, 2109004.

43 M. Rubinstein and R. H. Colby, *Polymer Physics*, Oxford University Press, Oxford, UK, 2003.

44 T. Çaykara, S. Demirci, M. S. Eroğlu and O. Güven, *Polymer*, 2005, **46**, 10750–10757.

45 D. Hill, Q. Tang, F. Fazelpour, M. Raihan, S. King, W. Kissner, C. Esther, B. Button, S. Danielsen and M. Rubinstein, *J. Cystic Fibrosis*, 2024, **23**, S118–S119.

46 M. Caldara, R. S. Friedlander, N. L. Kavanaugh, J. Aizenberg, K. R. Foster and K. Ribbeck, *Curr. Biol.*, 2012, **22**, 2325–2330.

47 C. Pawul, T. T. Dutta, S. G. Johnson and J. X. Tang, *Langmuir*, 2024, **40**, 27307–27313.

48 K. R. Bhaskar, D. Gong, R. Bansil, S. Pajevic, J. A. Hamilton, B. S. Turner and J. T. LaMont, *Am. J. Physiol.: Gastrointest. Liver Physiol.*, 1991, **261**, G827–G833.

49 D. J. Thornton and J. K. Sheehan, *Proc. Am. Thorac. Soc.*, 2004, **1**, 54–61.

50 H. Matsui, B. R. Grubb, R. Tarran, S. H. Randell, J. T. Gatzy, C. W. Davis and R. C. Boucher, *Cell*, 1998, **95**, 1005–1015.

51 C. L. Hattrup and S. J. Gendler, *Annu. Rev. Physiol.*, 2008, **70**, 431–457.

52 M. Kesimer, C. Ehre, K. A. Burns, C. W. Davis, J. K. Sheehan and R. J. Pickles, *Mucosal Immunol.*, 2013, **6**, 379–392.

53 C. L. Haley, C. Kruczek, U. Qaisar, J. A. Colmer-Hamood and A. N. Hamood, *Can. J. Microbiol.*, 2014, **60**, 155–166.

54 A. T. Y. Yeung, A. Parayno and R. E. W. Hancock, *mBio*, 2012, **3**, e00073-12.

55 J. C. Conrad, M. L. Gibiansky, F. Jin, V. D. Gordon, D. A. Motto, M. A. Mathewson, W. G. Stopka, D. C. Zelasko, J. D. Shrout and G. C. L. Wong, *Biophys. J.*, 2011, **100**, 1608–1616.

56 G. Li, L.-K. Tam and J. X. Tang, *Proc. Natl. Acad. Sci. U. S. A.*, 2008, **105**, 18355–18359.

57 M. D. Koch, M. E. Black, E. Han, J. W. Shaevitz and Z. Gitai, *Proc. Natl. Acad. Sci. U. S. A.*, 2022, **119**, 1–9.

58 A. Persat, Y. F. Inclan, J. N. Engel, H. A. Stone and Z. Gitai, *Proc. Natl. Acad. Sci. U. S. A.*, 2015, **112**, 7563–7568.

59 S. S. Webster, C. K. Lee, W. C. Schmidt, G. C. L. Wong and G. A. O'Toole, *Proc. Natl. Acad. Sci. U. S. A.*, 2021, **118**, 1–9.

60 M. C. Wolfgang, B. R. Kulasekara, X. Liang, D. Boyd, K. Wu, Q. Yang, C. G. Miyada and S. Lory, *Proc. Natl. Acad. Sci. U. S. A.*, 2003, **100**, 8484–8489.

61 E. Lauga, W. R. DiLuzio, G. M. Whitesides and H. A. Stone, *Biophys. J.*, 2006, **90**, 400–412.

62 P. D. Frymier, R. M. Ford, H. C. Berg and P. T. Cummings, *Proc. Natl. Acad. Sci. U. S. A.*, 1995, **92**, 6195–6199.

63 K. Maeda, Y. Imae, J. I. Shioi and F. Oosawa, *J. Bacteriol.*, 1976, **127**, 1039–1046.

64 P. D. Frymier and R. M. Ford, *AIChE J.*, 1997, **43**, 1341–1347.

65 K. Son, J. S. Guasto and R. Stocker, *Nat. Phys.*, 2013, **9**, 494–498.

66 V. A. Martinez, J. Schwarz-Linek, M. Reufer, L. G. Wilson, A. N. Morozov and W. C. K. Poon, *Proc. Natl. Acad. Sci. U. S. A.*, 2014, **111**, 17771–17776.

67 H. C. Berg and L. Turner, *Nature*, 1979, **278**, 349–351.

68 E. Lauga and T. R. Powers, *Rep. Prog. Phys.*, 2009, **72**, 096601.

69 J. Teran, L. Fauci and M. Shelley, *Phys. Rev. Lett.*, 2010, **104**, 1–4.

70 J. P. Celli, B. S. Turner, N. H. Afdhal, S. Keates, I. Ghiran, C. P. Kelly, R. H. Ewoldt, G. H. McKinley, P. So, S. Erramilli and R. Bansil, *Proc. Natl. Acad. Sci. U. S. A.*, 2009, **106**, 14321–14326.

71 S. Kamdar, S. Shin, P. Leishangthem, L. F. Francis, X. Xu and X. Cheng, *Nature*, 2022, **603**, 819–823.

72 A. L. Hook, J. L. Flewellen, J.-F. Dubern, A. M. Carabelli, I. M. Zaid, R. M. Berry, R. D. Wildman, N. Russell, P. Williams and M. R. Alexander, *mSystems*, 2019, **4**, e00390.

73 S. M. Vater, S. Weiße, S. Maleschlijski, C. Lotz, F. Koschitzki, T. Schwartz, U. Obst and A. Rosenhahn, *PLoS One*, 2014, **9**, e87765.

74 Q. Zhang, J. Li, J. Nijjer, H. Lu, M. Kothari, R. Alert, T. Cohen and J. Yan, *Proc. Natl. Acad. Sci. U. S. A.*, 2021, **118**, e2107107118.

75 A. Moreau, S. Mukherjee and J. Yan, *Isr. J. Chem.*, 2023, **63**, e202200075.

76 J. Yan, A. G. Sharo, H. A. Stone, N. S. Wingreen and B. L. Bassler, *Proc. Natl. Acad. Sci. U. S. A.*, 2016, **113**, E5337–E5343.

77 M. C. Rose, *Am. J. Physiol.: Lung Cell. Mol. Physiol.*, 1992, **263**, L413–L429.

78 D. J. Thornton, K. Rousseau and M. A. McGuckin, *Annu. Rev. Physiol.*, 2008, **70**, 459–486.

79 B. Huang, S. Nian and L.-H. Cai, *Sci. Adv.*, 2024, **3080**, 1–9.

80 Z. J. He, B. Huang and L. H. Cai, *ACS Nano*, 2024, **18**, 17586–17599.

81 L.-H. Cai, *Macromolecules*, 2025, **58**, 4320–4339.

82 A. G. Henderson, C. Ehre, B. Button, L. H. Abdullah, L.-H. Cai, M. W. Leigh, G. C. DeMaria, H. Matsui, S. H. Donaldson, C. W. Davis, J. K. Sheehan, R. C. Boucher and M. Kesimer, *J. Clin. Invest.*, 2014, **124**, 3047–3060.

83 B. Button, H. P. Goodell, E. Atieh, Y.-C. C. Chen, R. Williams, S. Shenoy, E. Lackey, N. T. Shenkute, L.-H. H. Cai, R. G. Dennis, R. C. Boucher and M. Rubinstein, *Proc. Natl. Acad. Sci. U. S. A.*, 2018, **115**, 12501–12506.

84 D. Ghosh and X. Cheng, *Phys. Rev. Res.*, 2022, **4**, 023105.

85 S. Ramaswamy, *Annu. Rev. Condens. Matter Phys.*, 2010, **1**, 323–345.

86 A. Be'er and G. Ariel, *Mov. Ecol.*, 2019, **7**, 9.

87 M. C. Marchetti, J. F. Joanny, S. Ramaswamy, T. B. Liverpool, J. Prost, M. Rao and R. A. Simha, *Rev. Mod. Phys.*, 2013, **85**, 1143–1189.

88 T. Bhattacharjee, D. B. Amchin, J. A. Ott, F. Kratz and S. S. Datta, *Biophys. J.*, 2021, **120**, 3483–3497.

89 O. Hallatschek, S. S. Datta, K. Drescher, J. Dunkel, J. Elgeti, B. Waclaw and N. S. Wingreen, *Nat. Rev. Phys.*, 2023, **5**, 407–419.

90 B. O. T. Maldonado, A. Théry, R. Tao, Q. Brosseau, A. J. T. M. Mathijssen and P. E. Arratia, *Proc. Natl. Acad. Sci. U. S. A.*, 2024, **121**, e2417614121.

91 S. Gonzalez La Corte, C. Stevens, G. Cárcamo-Oyarce, K. Ribbeck, N. Wingreen and S. Datta, *Sci. Adv.*, 2025, **11**, eadq7797.